THE JOURNAL OF PHYSICAL CHEMISTRY C

pubs.acs.org/JPCC Article

Role of Hydrogen-Related Defects in Photocatalytic Activity of ZnO Films Grown by Atomic Layer Deposition

Robert Peter,* Kresimir Salamon, Ales Omerzu, Joerg Grenzer, Ivana Jelovica Badovinac, Iva Saric, and Mladen Petravic*

Cite This: https://dx.doi.org/10.1021/acs.jpcc.0c01519 Read Online

ACCESS | Metrics & More | Article Recommendations | Supporting Information

ABSTRACT: The photocatalytic activity of ZnO films, grown by atomic layer deposition on sapphire, was investigated for different amounts of residual hydrogen incorporated unintentionally into the matrix during the crystal growth. A close correlation was found between the level of incorporated hydrogen and the rate of photocatalytic degradation of methylene blue on ZnO films. The rate of degradation is consistent with predominantly zero-order reaction kinetics. An enhanced photocatalytic activity, observed for films of predominantly (001)-oriented grains and low concentration of residual hydrogen, is explained by the reduced number of hydrogen-related defects responsible for recombination of charge carriers in combination with the preferential adsorption of water on polar (001) surfaces of ZnO grains.

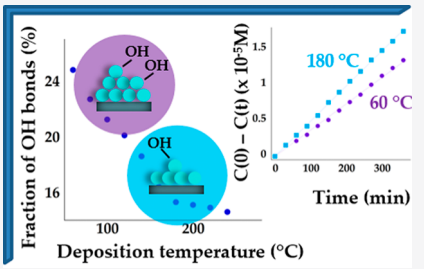

INTRODUCTION

Zinc oxide (ZnO) is a direct band gap II−VI semiconductor with a wide range of attractive physical and chemical properties, including a direct band gap of 3.37 eV, a large exciton binding energy of 60 meV, the high transparency in visible and near-ultraviolet spectral regions, low electrical resistivity, high piezoelectric constants, biocompatibility, and high chemical and thermal stability.[1,2] It has been, therefore, recognized as a promising material for applications in a large variety of electronic and optoelectronic devices, from the light-emitting diodes, photodetectors,[3,4] or field-effect transistors[5] to the piezoelectric transducers,[6] gas sensors,[4] or solar cells,[7] and acoustic wave devices.[8,9]

In addition, ZnO has been widely studied over the past decade as an alternative photocatalytic material to standard photocatalysts, such as TiO_2, WO_3, or Fe_2O_3,[10] or some hybrid nanomaterials functionalized with nanoparticles,[11] to mention just a few. In general, photocatalysis starts with the photogeneration of electrons and holes in the material and their transport to the surface, where they produce hydroxyl and superoxide radicals from water and oxygen, respectively, adsorbed at the photocatalyst surface. These radicals initiate redox reactions at the surface.[10,12] However, the charge carriers can rapidly recombine directly or at the trapping sites at the surface or within the bulk, resulting in low reactivity. In addition, the efficiency of redox processes depends on the number of reactive sites at the surface, that is, on the active surface area, and on the wettability of surface (preferential adsorption of water and contaminants on the surface).[10] Therefore, the improvement of the photocatalytic process involves the optimization of several mechanisms, from the generation and separation of charge carriers to their trapping and recombination with the increase of surface-active area and wettability.

The most common recombination sites in semiconducting polycrystalline films are interstitial atoms, vacancies, or grain boundaries. These defects can create deep or shallow states within the energy gap, affecting trapping and recombination of electrons and holes and, therefore, deteriorating the photocatalytic activity at the surface.[10,12] The creation of defects, as well as the development of a different surface morphology, depends on the material's growth conditions. Therefore, the general strategy for the growth conditions should comprise at least three requirements: (i) reducing the number of defect sites, (ii) generating an appropriate morphology of the surface with a high specific area that will provide a great number of reactive sites for increased adsorption of water and pollutants, and (iii) providing a surface texture (preferential orientation of crystal grains) with high wettability.

In the present paper, we explore the above three requirements in order to maximize the photocatalytic activity of thin ZnO films, with nanosize granular structures, grown by atomic layer deposition (ALD). Previously, some other nanostructures of ZnO, such as nanoparticles and nanowires, were also studied for improved photocatalytic applications. For example, one obvious advantage of nanoparticles is their large active surface area, which, however, can be greatly reduced

Received: February 21, 2020
Revised: March 27, 2020
Published: March 30, 2020

because of the ease of agglomeration of nanoparticles in solutions. In addition, a post-treatment is usually required to remove the nanoparticle catalyst from the solution, while complete recovery of catalyst is quite difficult. On the other hand, nanofilms of ZnO could also provide a large active surface area (because of the nanosized grains) and can be deposited on most substrates, and no post-treatment is required while the films are almost completely recovered after the photocatalytic process.[13]

Various deposition techniques have been used to grow high-quality ZnO films for photocatalytic applications, including molecular beam epitaxy, metalorganic chemical vapor deposition, pulsed laser deposition, radiofrequency magnetron sputtering, ion beam sputtering, or ALD.[14−20] Among them, ALD possesses several unique features. It is characterized by monolayer-by-monolayer growth of thin films, where precursors containing elements of the final film chemically react at the very surface of the substrate, followed by the removal of the excess reactants from the processing chamber. In this way, the growth process is self-limiting and allows an accurate control of film thickness. Some other practical advantages of ALD include excellent conformity, high uniformity over a large area, and good reproducibility.[21] In addition, the high chemical reactivity of precursors used in ALD allows deposition of ZnO films at considerably lower temperatures compared with temperatures applied in some other deposition techniques, which are often above 500 °C.[22] Indeed, the high quality polycrystalline ZnO films have been deposited by ALD at temperatures as low as 100 °C.[23,24]

Native defects in the ZnO crystal lattice include mostly vacancies, antisites, and interstitials. Among them, oxygen vacancies, V_O, and zinc interstitials, Zn_i, have been considered as sources of n-type conductivity of ZnO, while zinc vacancies, V_{Zn}, have been identified as the main compensating centers in n-type ZnO.[2] In addition, V_{Zn} is the most stable defect in ZnO, having, at the same time, the lowest formation energy of all native defects.[2,25] Therefore, one expects the formation of at least modest concentrations of V_{Zn} during the ALD growth of ZnO. On the other hand, the as-grown ALD films are always contaminated unintentionally with a large amount of impurities,[26,27] especially with hydrogen that is unavoidably present in all techniques used for the growth or the modification of ALD films and which can easily penetrate into any host matrix. For example, both precursors used in ALD growth of ZnO contain a considerable amount of hydrogen. In ZnO, hydrogen atoms can either occupy interstitial sites or form very stable V_{Zn}-H complexes.[2,25,28] H atoms are bonded to V_{Zn} through the formation of strong O−H bonds.[25] The presence of OH and H bonds in ZnO was found previously to promote the recombination of charge carriers on ZnO surfaces.[29]

On the other hand, ALD synthesis of ZnO usually results in polycrystalline wurtzite films, where the texture (preferential orientation of the ZnO grains) strongly depends on the growth conditions and the type of the substrate.[30] Therefore, controlling the crystal growth direction is of crucial importance for photocatalytic applications of ZnO. At the same time, the ZnO texture can influence some other chemical and physical properties of the material. For instance, the (001) orientated grains are needed for a good piezoelectric activity of the ZnO,[6,8,9] while ZnO films with (100) or (110) textures provide high conductivity and are suitable for transparent conductive oxide applications.[22,31]

For the present study, ZnO films with different textures and concentrations of residual hydrogen were grown by ALD on sapphire substrates. The selection of appropriate substrates is critical as it controls the properties of the synthesized material.[32,33] The advantages of sapphire substrates for the ZnO growth are low cost and the high crystalline perfection of large sapphire wafers, while the relatively large lattice mismatch to ZnO of about 18% does not prevent the growth of high quality ALD films.[22] In addition, the wurtzite (001) sapphire plane has the highest atomic packing density and the minimum surface free energy,[34] making the growth of ZnO with the *c*-axis perpendicular to the sapphire surface thermodynamically favorable.

The elemental composition and the relative fraction of hydrogen bonds in the deposited films were determined in the present study from secondary ion mass spectrometry (SIMS) and X-ray photoemission spectroscopy (XPS) measurements, while SIMS was also used for the in-depth uniformity and film thickness measurements. The surface morphology was monitored by scanning electron microscopy (SEM). The crystalline structure of all films was obtained by X-ray diffraction (XRD) measurements. The photocatalytic activity of ZnO films was evaluated from the degradation rate of methylene blue (MB) in an aqueous solution under the UV illumination.

EXPERIMENTAL SECTION

The growth of ZnO films on (001) oriented sapphire substrates, c-Al_2O_3 (Semiconductor Wafer Inc.), was carried out in a Beneq TFS 200 system. Diethylzinc (DEZ, $Zn(C_2H_5)_2$) and distilled water (H_2O) were used as zinc and oxygen precursors, respectively. Prior to the deposition, the sapphire substrates were ultrasonically cleaned in acetone, distilled water, and isopropanol and dried with N_2 gas. One growth cycle consisted of 180 ms pulse of DEZ, followed by 1 s purge with high-purity nitrogen (purity 6.0), 180 ms pulse of H_2O, with the final purging step with N_2 for 1 s. The number of ALD cycles was kept fixed at 450 for all deposition temperatures, giving the films thickness within the range of 80 ± 20 nm. In the present study, we focus on the photocatalysis on samples grown within the temperature range of 60−180 °C, where a significant change in the level of incorporated hydrogen was detected.

The XPS analysis was carried out in a SPECS instrument equipped with a Phoibos MCD 100 electron analyzer and a monochromatized source of Al K_α X-rays of 1486.74 eV. The spectra, recorded with an electron pass energy of 10 eV, were deconvoluted using mixed Gaussian−Lorentzian functions with Shirley background subtraction.[35] The binding energy (BE) scale of XPS spectra was calibrated by the reference carbon C 1s peak, adjusted to the BE of 285.0 eV.

A Hiden SIMS workstation, equipped with the quadrupole mass analyzer, was employed for the SIMS measurements, where the bombardment with 3 keV O_2^+ or 5 keV Cs^+ primary ions at an impact angle of 45° were used for the collection of secondary ions. The depth of all SIMS craters was measured with a Dektak XT stylus surface profiler.

The surface morphology was imaged using a Jeol JSM-7800F SEM in a surface-sensitive gentle beam mode with an electron accelerating voltage of 0.7 kV. The crystalline structure was established from XRD measurements using a Siemens D5000 diffractometer with Cu K_α radiation and a Goebel mirror in conventional $\theta-2\theta$ geometry. The in-plane

https://dx.doi.org/10.1021/acs.jpcc.0c01519
J. Phys. Chem. C XXXX, XXX, XXX−XXX

and out-of-plane relationships between the ZnO epilayers and the substrate were determined by measuring the pole figures at the (101) and (002) ZnO reflections. The pole figure measurements were performed using a 4-circle-θ-θ diffractometer (Empyrean/Panalytical) in parallel beam geometry with Cu K_α radiation, a point detector, and a collimator in front of the detector.

Finally, the photocatalytic activity of ZnO films was evaluated from the degradation rate of MB solution under UV irradiation for different times (0−6 h). The ZnO samples of 2 cm × 1 cm were dipped into a water solution of MB of initial concentration of 3.5×10^{-5} M (where M is the molar concentration in mol/L or mol/dm^3) and irradiated using a UV lamp of 254 nm and 6 W. The absorption spectrum of the MB solution was taken every 30 min using a UV−Vis spectrophotometer (Thermo Scientific, Evolution 201), monitoring the change in intensity of the characteristic absorbance peak of MB at 664 nm.

RESULTS AND DISCUSSION

The high level of residual hydrogen, unintentionally introduced during the ALD growth of ZnO films, is expected in all samples as both ALD precursors used in this study, DEZ and H_2O, contain hydrogen. In ZnO, hydrogen either occupies interstitial sites or forms very stable V_{Zn}-H complexes, by forming strong bonds with oxygen. In both cases, the chemical shift in the XPS spectra around the O 1s core-level could indicate the presence of hydrogen (i.e., the presence of O−H bonds).[36] Photoemission spectra around the O 1s level, for the samples grown at 60 and 180 °C are shown in Figure 1. Prior

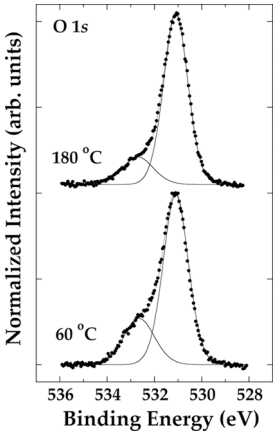

Figure 1. Photoemission spectra around O 1s core-levels for samples grown at 60 and 180 °C. Experimental curves are represented by closed circles, while solid lines represent a numerical fit (mixture of Gaussian and Lorentzian functions).

to the XPS measurement, the samples were exposed to the 1 keV Ar^+ ion bombardment for 5 min within the analytical chamber of the XPS instrument, in order to remove carbon or residual gases adsorbed on the surface during exposure of ZnO samples to the atmosphere.

Both spectra exhibit a distinctive structure, deconvoluted into two components: the main peak at the BE of 531.1 eV was assigned to the photoemission from O^{2-} ions of the Zn−O bonds in the ZnO matrix,[37,38] while the less intensive feature located at BE of 532.7 eV has been assigned previously to the photoemission from oxygen in Zn−OH or OC bonds.[37,38] As the C 1s signal was not observed in XPS survey spectra (see Figure S1 of Supporting Information), we rule out the presence of O−C bonds in the O 1s photoemission from Figure 1 and assign the smaller peak to the OH bonds. At the same time, the photoemission around Zn 2p core-levels does not exhibit any changes with the processing temperature (see Figure S2 of the Supporting Information).

With the increase of the deposition temperature from 60 to 180 °C, the relative intensity of the OH-related peak decreases (see Figure 1), clearly indicating the reduction of OH species in samples grown at higher deposition temperatures. In order to quantify the amount of hydrogen impurities, we plotted in Figure 2 the relative concentration of the OH-related peaks as

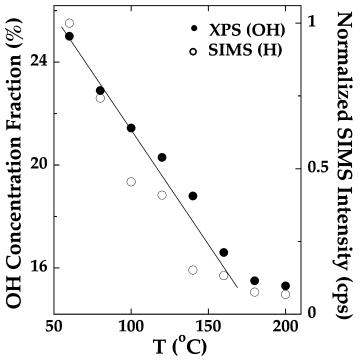

Figure 2. Relative fraction of OH bonds extracted from XPS measurements (closed circles) and normalized intensity of the H signal from SIMS measurements (open circles) as a function of deposition temperature. Error bars are within the size of symbols. Solid line is a guide for the eye.

a function of deposition temperature. The concentration fraction of H-related peak (closed circles in Figure 2) is decreasing almost linearly with the deposition temperature up to 180 °C and exhibits no significant changes above that temperature. A significant 40% reduction in relative hydrogen content is observed in XPS when changing the deposition temperature from 60 to 200 °C.

The stoichiometry of ZnO films does not change significantly with the deposition temperature. The ratio of Zn/O atoms (obtained from the XPS spectra) is close to 1 for all samples grown between 100 and 160 °C, with some slightly lower values for the lower deposition temperatures (see Figure S3 of the Supporting Information).

We supplement the XPS measurements with SIMS in-depth profiles of hydrogen. Typical SIMS in-depth profiles of hydrogen, zinc, oxygen, and aluminum, together with the profile of OH molecules, are shown in Figure 3 for a film grown at 60 °C. The concentrations of Zn and O atoms are quite constant throughout the film, with a sharp interface between the ZnO film and the sapphire substrate (represented in SIMS profiles by the Al signal). Constant and high SIMS yield of H and OH ions throughout the film indicates an efficient incorporation of H atoms into the matrix. In Figure 2, we also show the intensity of the H signal from SIMS measurements on all ZnO films, normalized to the Zn signal (open circles in Figure 2). Without proper standard samples, it is not possible to extract atomic concentration of hydrogen from SIMS profiles. Therefore, Figure 2 displays only the qualitative changes of hydrogen concentration with the deposition temperature. However, a clear correspondence exists between XPS and SIMS measurements, as shown in

https://dx.doi.org/10.1021/acs.jpcc.0c01519
J. Phys. Chem. C XXXX, XXX, XXX−XXX

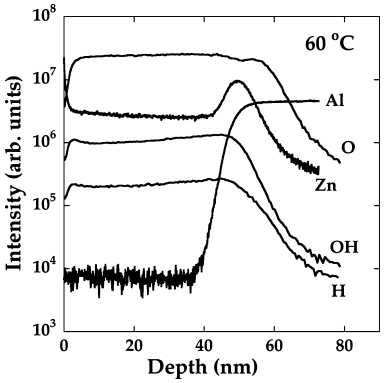

Figure 3. SIMS in-depth profile of a ZnO film grown at 60 °C.

Figure 2. We also note the difference in relative change of OH and H signals. While the relative OH concentration fraction obtained by XPS changes by a factor of 1.7 between the lowest and the highest deposition temperatures in Figure 2, the intensity of the SIMS signal changes by a factor of 14. Therefore, it seems that only a fraction of incorporated hydrogen atoms is engaged in the O−H bonding.

We turn now to the analysis of the crystal structure of ZnO samples by investigating their surface morphology by SEM. Figure 4 shows several representative SEM micrographs of

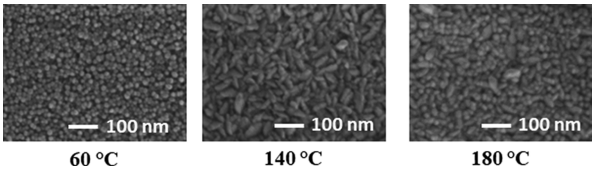

Figure 4. SEM micrographs of samples grown at deposition temperatures of 60, 140, and 180 °C.

ZnO films grown at 60, 140, and 180 °C. All films show compact, granular structures with some obvious differences in the size and the shape of the ZnO grains. The film grown at the lowest deposition temperature has cylindrical and columnar crystallites. The surface morphology changes in films deposited at the temperatures above 100 °C, with the development of wedge-shaped crystallites that are mixed with the columnar grains. The cylindrical and columnar crystallites dominate again the structure at higher temperatures (above 160 °C), as shown in Figure 4, for a sample grown at 180 °C.

The surface morphology of ZnO films deposited at different temperatures is related to the grain orientations within the films. Figure 5 shows the characteristic $\theta-2\theta$ XRD patterns of ZnO films grown at 60, 140, and 180 °C together with the calculated pattern of the randomly oriented ZnO wurtzite crystallites. The $\theta-2\theta$ scans already reveal strongly textured films, as only 002 and 101 reflections are visible in the spectra. All ZnO films examined in the present study show crystallites having (001) and (101) planes parallel to the substrate surface. Indeed, the most common crystal orientation for ZnO films grown by ALD on sapphire is the (001) orientation,[32,39,40] while some studies report on the mixture of (001) with some other orientations, such as (101),[23,32,41] (111),[41] or (100).[42] From the width of 002 reflections (see Figure 5), we have determined the out-off-plane crystallite size of 16−25 nm. These values are slightly lower than the average grain size of 20−35 nm, as estimated from the SEM images.

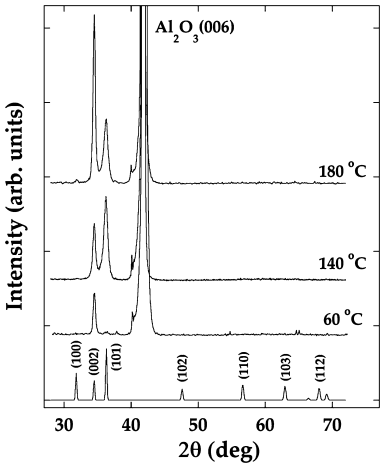

Figure 5. $\theta-2\theta$ XRD patterns of ZnO films deposited at 60, 140, and 180 °C. Calculated XRD pattern for ZnO powder is shown at the bottom.

In order to quantify the texture, we determined the fractions of (001) and (101) textures for each film, by comparing the relative intensities of measured and calculated 002 and 101 reflections, respectively. A strong dependence of the texture fraction on the deposition temperature is found, as shown in Figure 6. The preferential orientation of grains changes from

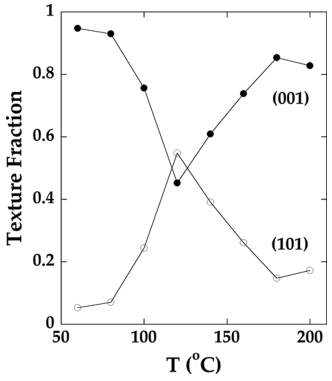

Figure 6. (101) and (001) ZnO texture fractions as a function of deposition temperature taking into account normalized peak intensities. Solid line is a guide for the eye.

(001) for samples grown at lower deposition temperatures to the mixture of (001) and (101) oriented grains at intermediate temperatures (100−150 °C) and back to the dominance of (001)-grains at temperatures above 150 °C. The morphology of films observed with SEM is consisted with the texture fraction: the (001) texture is dominant in films with the columnar crystallites, while the films with a higher fraction of (101) texture show more wedge-shaped crystallites.

Interestingly enough, the films grown at 120−200 °C show a strong in-plane ordering of the ZnO grains. The in-plane epitaxial relationship between the ZnO film and the sapphire substrate was extracted from the pole figure measurements. Briefly, we show in Figure 7 the representative (002) and (101) pole figures for the film grown at 180 °C. All maxima appearing in the pole figures can be explained with the (001) and (101) preferred orientations (red circles and blue squares in Figure 7, respectively), confirming that the other possible orientations are not present in the films, in full agreement with

https://dx.doi.org/10.1021/acs.jpcc.0c01519
J. Phys. Chem. C XXXX, XXX, XXX−XXX

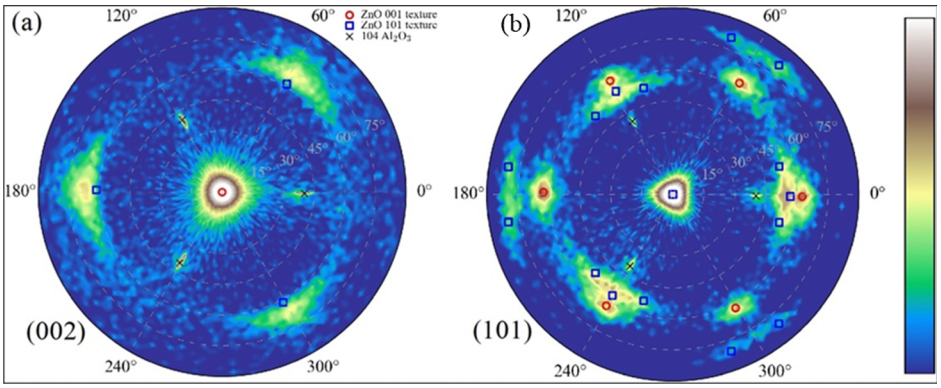

Figure 7. ZnO (002) and (101) pole figures for a film grown at 180 °C. The maxima are indexed with red circles or blue squares corresponding to the reflections originating from (001) and (101) textures of ZnO, respectively. The 104 Al_2O_3 substrate reflections are denoted by black crosses.

the $\theta-2\theta$ measurements of Figure 5. In addition, the epitaxial relationships between the substrate and the film can be determined from (104) reflections from the c-Al_2O_3 substrate (denoted with black crosses in Figure 7). More details are given in Supporting Information (Figure S4).

Turning now to the photocatalytic activity of ZnO films, we recall that the degradation rate, r, of water solution of pollutant molecules of concentration C (MB in our case) can be given by the differential rate equation

$$r = -\mathrm{d}[C]/\mathrm{d}t = k[C]^n \quad (1)$$

where k is the rate constant and n is the order of reaction.[12] The solutions of eq 1 for the zero order reaction ($n = 0$) and the first order reaction ($n = 1$) are

$$C_t = C_0 - kt \quad (2)$$

and

$$C_t = C_0 \exp(-kt) \quad (3)$$

respectively, where t is the exposure time of MB solution to UV and C_0 and C_t are the initial and the instantaneous concentration of MB solution, respectively. Therefore, a plot of C_t against t gives a straight line for a zero order reaction, with slope equals $-k$ and intercept equals C_0. Similarly, the rate constant for a first order reaction is determined from the slope of a $\ln(C_t/C_0)$ versus t straight line, with intercept equalling zero.

The degradation rate of water solution of MB, measured in the present study on ZnO surfaces grown at 60, 100, 140, and 180 °C, is better described by the zero order reaction, as shown in Figure 8, for a lin−lin plot of $C_0 - C_t$ as a function of the UV exposure time, t (given in minutes), for ZnO samples grown at 60, 140, and 180 °C, respectively (for the clarity of presentation, only results for three temperatures are shown in Figure 8). As expected from the eq 2, the plot gives a straight line whose intercept equals 0 and slope equals $-k$ (we note that for a zero order reaction, the unit of k is M min^{-1}). The linear fitting deviation is given by the correlation factor R^2 that is close to 1 for fittings, as in Figure 8, strongly supporting the linear relationship between C_t and t, that is, the dominance of the zero order photocatalytic kinetics. The values of rate constants normalized to the active surface of ZnO films are 7.56×10^{-8}, 8.10×10^{-8}, 8.20×10^{-8}, and 11.24×10^{-8} M min^{-1} cm^{-2} for 60, 100, 140, and 180 °C, respectively. For comparison, we show in Supporting Information, Figure S5,

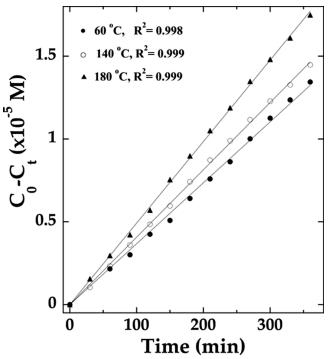

Figure 8. Change in concentration of MB solution, $C_0 - C_t$, as a function of time exposure to UV light for the films grown at 60 °C (closed circles), 140 °C (open circles), and 180 °C (closed triangles). R^2 is the correlation factor for the linear fitting of the experimental data.

the corresponding $\ln(C_t/C_0)$ versus t curves, clearly exhibiting much worse correlation factors for the linear fittings.

The zero order kinetics is characteristic for photocatalytic reactions in which the degradation rate does not change with the concentration of pollutants (water solution of MB in the present study). In other words, the pollutant is in large excess and the catalyst surface is completely covered by the pollutant. At such saturation coverage, any change in the concentration does not influence the photocatalytic kinetics.[43] While the most photocatalytic data on ZnO in literature were analyzed using the first order kinetics,[44,45] there are several reports on the zero order reactions for different photocatalytic materials, including TiO_2,[46] $SrTiO_3$,[47] or Fe_3O_4.[48]

In order to explain the improved photocatalytic efficiency at higher deposition temperatures (see Figure 8), we point first at the increase in efficiency of about 30% for films grown at 180 °C, compared to films grown at 60 °C, although both films are showing the dominance of (001)-oriented grains [with 60 °C-film exhibiting even slightly a higher concentration of (001)-grains]. This observation contradicts the well-established behavior of photocatalytic activity of ZnO thin films and nanostructures, which exhibit the highest photocatalytic activity for (001)-oriented grains,[44,49−51] namely, the high absorption rate of water on polar (001) planes generates the contact of more pollutants with the active sites on the surface, resulting in the higher degradation rate of pollutants in aqueous solution.[44,49−51] However, comparison of results presented in Figures 6 and 8, clearly demonstrates that a

https://dx.doi.org/10.1021/acs.jpcc.0c01519
J. Phys. Chem. C XXXX, XXX, XXX−XXX

higher photocatalytic activity (up to 30% as found in the present study) can be achieved on films with a lower fraction of (001)-oriented grains. Therefore, some other competing processes within the ZnO films determine the low photocatalytic activity of films grown at low deposition temperatures. We recall here a recent study[45] suggesting that hydrogen impurities can influence the photocatalytic properties of ZnO thin films. The strong dependence of the residual H concentration on the deposition temperature found in the present study (see Figure 2) supports this suggestion. We argue that H-related defects, such as interstitial hydrogen or islands of amorphous ZnO_xH_y phases within the crystalline ZnO matrix,[45] may act as trapping and recombination centers for charge carriers. Consequently, the number of free charge carriers reaching the surface of ZnO is reduced, reducing in turn the production of chemically highly reactive hydroxyl and superoxide radicals, essential for decomposing MB to carbon dioxide, water, and mineral acids.[10] The film grown at 60 °C contains the largest amount of H-induced defects, decreasing the photocatalytic efficiency of this film despite the highest fraction of (001)-oriented grains on the surface. Obviously, the high concentration of trapping/recombination sites in this case overcomes the benefit of a high absorption rate for water. On the other hand, although a lower fraction of (001) grains grown at higher temperatures reduces slightly the water absorption efficiency, this reduction is compensated with the lower concentration of hydrogen-related defects, leading to the higher photocatalytic efficiency of films grown at higher temperatures.

Finally, we consider several types of hydrogen-related defects in the ZnO matrix that might be responsible for the observed changes in photocatalytic activity. As already mentioned, there are several possible sites for the incorporation of hydrogen atoms into the ZnO matrix: (i) they can be placed at interstitial positions, (ii) they can form V_{Zn}-H complexes, or (iii) they can be incorporated into the segregated amorphous ZnO_xH_y phase.[2,25,28,45] The existence of interstitial H or V_{Zn}-H complexes in ZnO has been found previously to change the lattice parameters,[2,52] while the existence of a ZnO_xH_y phase may cause a small chemical shift in the XPS spectra around Zn 2p levels related to the formation of Zn−OH bonds.[53] As no detectable changes have been observed in the Zn 2p photoemission peaks (See Figure S2 in Supporting Information), we argue that large islands of amorphous ZnO_xH_y are not likely to form in samples examined in the present study.

On the other hand, the ZnO lattice parameter *c*, extracted from the 002 diffraction peaks of the θ–2θ scans, seems to depend on processing temperature in the same qualitative way as the SIMS intensity of the H signal (see Figure 9). The changes in the lattice parameter *c* are small but measurable and reproducible, as checked by two sets of films grown on c-Al_2O_3 substrates and one set of films on SiO_2 substrates grown simultaneously together with the sapphire substrates. The data are shown in Figure 9. The value of *c* decreases from around 5.230 ± 0.005 Å for films grown at 60 °C to a saturation value of around 5.195 ± 0.005 Å for films grown above 150 °C. In the same figure, we display once again the normalized SIMS intensity of the H signal (related to the hydrogen concentration in ZnO; open circles in Figure 9). An obvious correlation exists between the lattice distortion and the concentration of hydrogen in ZnO films. This is a strong indication that hydrogen atoms participate in the ZnO lattice

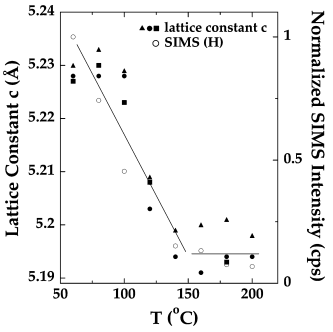

Figure 9. Lattice constant, *c*, extracted from the XRD measurements as a function of deposition temperature, taken from two sets of ZnO samples grown on sapphire (closed squares and closed circles) and one set grown simultaneously on SiO_2 (closed triangles). Open circles represent normalized SIMS intensity of the H signal. Solid line is a guide for the eye.

as interstitial defects, stretching the lattice, and, at the same time, deteriorating the photocatalytic efficiency at lower deposition temperatures (see Figure 8). We stress here once again that the *c* parameter was determined from the 002 diffraction peak corresponding to the (001) oriented grains, assuming the same incorporation rate of hydrogen into crystallites of different orientations.

The comparison of XPS and SIMS measurements from Figure 2, that is, the relative concentration of O−H bonds and H atoms, respectively, indicates that the most H atoms incorporated during the crystal growth are placed at the interstitial positions. However, we argue that a fraction of H atoms is involved in formation of highly stable complexes with V_{Zn} in which the vacancy can bind one or two H atoms.[25] In addition, H atoms form strong bonds with the nearest O atom. Hydrogenated Zn vacancies are very stable and are unlikely to dissociate after formation.[25] The presence of O−H bonds was found to play an important role in electron−hole recombination in several semiconductors, including Zn surfaces,[29] n-type Si,[54] or Ta_3N_5.[55] The present study, indeed, confirms the close correlation between the relative concentration of O−H bonds and the photocatalytic efficiency of ZnO related to the recombination of charge carriers.

CONCLUSIONS

In conclusion, we examined the influence of residual hydrogen on the photocatalytic activity of ZnO films grown by ALD at different temperatures. The concentration of hydrogen atoms, introduced unintentionally during the ALD growth, decreases with the processing temperature as measured by SIMS. At the same time, the relative fraction of OH bonds, obtained by XPS measurements, shows similar behavior, although with significantly a lower total change, indicating that only a fraction of incorporated hydrogen is engaged in O−H bonds. We argue that hydrogen atoms are either incorporated at interstitial positions or form very stable V_{Zn}-H complexes with H atoms bonded to V_{Zn} through the formation of strong O−H bonds. A higher level of hydrogen, occupying interstitial sites in ZnO at lower deposition temperatures, slightly stretching the lattice parameter *c*, is in full agreement with our measurements. On the other hand, the presence of V_{Zn}-H complexes in ZnO promotes the recombination of charge carriers, thus degrading the photocatalytic activity of ZnO films, again in full agreement with our measurements for films grown at lower temperatures.

https://dx.doi.org/10.1021/acs.jpcc.0c01519
J. Phys. Chem. C XXXX, XXX, XXX−XXX

An enhanced photocatalytic activity was observed for films satisfying two conditions: the reduced number of hydrogen-related V_{Zn}-H defects, responsible for the recombination of charge carriers, and the dominance of (001)-oriented grains in ZnO films, responsible for the preferential adsorption of water. The rate of degradation of MB is best described by the zero order reaction kinetics. In other words, the water solution of MB used in the present study completely covers the active sites on the ZnO surface.

■ ASSOCIATED CONTENT

Supporting Information

The Supporting Information is available free of charge at https://pubs.acs.org/doi/10.1021/acs.jpcc.0c01519.

XPS survey spectra from two ZnO samples grown at two different temperatures, photoemission around the Zn 2p core level, Zn/O atomic ratio as a function of processing temperature, in-plane epitaxial relationship between the ZnO film and the sapphire substrate extracted from the pole figures measurements, and lin−log plot of the MB degradation (PDF)

■ AUTHOR INFORMATION

Corresponding Authors

Robert Peter − *Department of Physics and Center for Micro- and Nanosciences and Technologies, University of Rijeka, 51000 Rijeka, Croatia;* orcid.org/0000-0002-5669-1985; Phone: +385-51-584621; Email: rpeter@uniri.hr; Fax: +385-51-584649

Mladen Petravic − *Department of Physics and Center for Micro- and Nanosciences and Technologies, University of Rijeka, 51000 Rijeka, Croatia*; Phone: +385-51-584622; Email: mpetravic@uniri.hr; Fax: +385-51-584649

Authors

Kresimir Salamon − *Ruder Boskovic Institute, 10000 Zagreb, Croatia*

Ales Omerzu − *Department of Physics and Center for Micro- and Nanosciences and Technologies, University of Rijeka, 51000 Rijeka, Croatia*

Joerg Grenzer − *Institute of Ion Beam Physics and Materials Research, Helmholtz-Zentrum Dresden-Rossendorf e.V., 01328 Dresden, Germany*

Ivana Jelovica Badovinac − *Department of Physics and Center for Micro- and Nanosciences and Technologies, University of Rijeka, 51000 Rijeka, Croatia;* orcid.org/0000-0001-7911-7380

Iva Saric − *Department of Physics and Center for Micro- and Nanosciences and Technologies, University of Rijeka, 51000 Rijeka, Croatia;* orcid.org/0000-0001-8509-3223

Complete contact information is available at: https://pubs.acs.org/10.1021/acs.jpcc.0c01519

Notes

The authors declare no competing financial interest.

■ ACKNOWLEDGMENTS

This study was supported by the Croatian Science Foundation under project IP-2016-06-3568, the European Fund for Regional Development and the Ministry of Science and Education of the Republic of Croatia under the grant number RC.2.2.06-0001 and the University of Rijeka under the project number 18-144.

■ REFERENCES

(1) *Zinc Oxide Bulk, Thin Films, and Nanostructures*; Jagadish, C., Pearton, S. J., Eds.; Elsevier: New York, 2006.

(2) Janotti, A.; Van de Walle, C. G. Fundamentals of Zinc Oxide as a Semiconductor. *Rep. Prog. Phys.* **2009**, *72*, 126501.

(3) Jung, B. O.; Kwon, Y. H.; Seo, D. J.; Lee, D. S.; Cho, H. K. Ultraviolet Light Emitting Diode Based on p-NiO/n-ZnO Nanowire Heterojunction. *J. Cryst. Growth* **2013**, *370*, 314−318.

(4) Shaikh, S. K.; Ganbavle, V. V.; Inamdar, S. I.; Rajpure, K. Y. Multifunctional Zinc Oxide Thin Films for High Performance UV Photodetectors and Nitrogen Dioxide Gas Sensors. *RSC Adv.* **2016**, *6*, 25641−25650.

(5) Zong, X.; Zhu, R. Zinc Oxide Nanorod Field Effect Transistor for Long-Time Cellular Force Measurement. *Sci. Rep.* **2017**, *7*, 43661.

(6) Nour, E. S.; Nur, O.; Willander, M. Zinc Oxide Piezoelectric Nano-generators for Low Frequency Applications. *Semicond. Sci. Technol.* **2017**, *32*, 064005.

(7) Pietruszka, R.; Witkowski, B. S.; Gieraltowska, S.; Caban, P.; Wachnicki, L.; Zielony, E.; Gwozdz, K.; Bieganski, P.; Placzek-Popko, E.; Godlewski, M. New Efficient Solar Cell Structures Based on Zinc Oxide Nanorods. *Sol. Energy Mater. Sol. Cells* **2015**, *143*, 99−104.

(8) Magnusson, E. B.; Williams, B. H.; Manenti, R.; Nam, M.-S.; Nersisyan, A.; Peterer, M. J.; Ardavan, A.; Leek, P. J. Surface Acoustic Wave Devices on Bulk ZnO Crystals at Low Temperature. *Appl. Phys. Lett.* **2015**, *106*, 063509.

(9) Serhane, R.; Abdelli-Messaci, S.; Lafane, S.; Khales, H.; Aouimeur, W.; Hassein-Bey, A.; Boutkedjirt, T. Pulsed Laser Deposition of Piezoelectric ZnO Thin Films for Bulk Acoustic Wave Devices. *Appl. Surf. Sci.* **2014**, *288*, 572−578.

(10) Kisch, H. *Semiconductor Photocatalysis: Principles and Applications*; Wiley-VCH: Weinheim, 2015.

(11) El Rouby, W. M. A.; Comesaña-Hermo, M.; Testa-Anta, M.; Carbó-Argibay, E.; Salgueiriño, V.; Pérez-Lorenzo, M.; Correa-Duarte, M. A. Au-decorated Sodium Titanate Nanotubes as High-Performance Selective Photocatalysts for Pollutant Degradation. *J. Phys. D: Appl. Phys.* **2017**, *50*, 144002.

(12) Gaya, U. I. *Heterogeneous Photocatalysis Using Inorganic Semiconductor Solids*; Springer: Dordrecht, 2014.

(13) Zhang, Y.; Ram, M. K.; Stefanakos, E. K.; Goswami, D. Y. Synthesis, Characterization, and Applications of ZnO Nanowires. *J. Nanomater.* **2012**, *2012*, 1−22.

(14) Chen, Y.; Bagnall, D. M.; Koh, H.-j.; Park, K.-t.; Hiraga, K.; Zhu, Z.; Yao, T. Plasma Assisted Molecular Beam Epitaxy of ZnO on c-plane Sapphire: Growth and Characterization. *J. Appl. Phys.* **1998**, *84*, 3912−3918.

(15) Ohkubo, I.; Matsumoto, Y.; Ohtomo, A.; Ohnishi, T.; Tsukazaki, A.; Lippmaa, M.; Koinuma, H.; Kawasaki, M. Investigation of ZnO/Sapphire Interface and Formation of ZnO Nanocrystalline by Laser MBE. *Appl. Surf. Sci.* **2000**, *159−160*, 514−519.

(16) Zhang, B. P.; Wakatsuki, K.; Binh, N. T.; Usami, N.; Segawa, Y. Effects of Growth Temperature on the Characteristics of ZnO Epitaxial Films Deposited by Metalorganic Chemical Vapor Deposition. *Thin Solid Films* **2004**, *449*, 12−19.

(17) Fanni, L.; Aebersold, B. A.; Alexander, D. T. L.; Ding, L.; Morales Masis, M.; Nicolay, S.; Ballif, C. C-texture Versus a-texture Low Pressure Metalorganic Chemical Vapor Deposition ZnO Films: Lower Resistivity Despite Smaller Grain Size. *Thin Solid Films* **2014**, *565*, 1−6.

(18) Wang, Y.-G.; Ohashi, N.; Wada, Y.; Sakaguchi, I.; Ohgaki, T.; Haneda, H. Lowering of Stimulated Emission Threshold of Zinc Oxide by Doping with Thermally Diffused Aluminum Supplied from Sapphire Substrate. *J. Appl. Phys.* **2006**, *100*, 023524.

(19) Abouzaid, M.; Ruterana, P.; Liu, C.; Morkoç, H. Atypical Grain Boundaries in ZnO Layers Deposited on Sapphire by rf Magnetron Sputtering on (0001) Sapphire. *Superlattices Microstruct.* **2007**, *42*, 110−115.

(20) Kennedy, J.; Murmu, P. P.; Leveneur, J.; Markwitz, A.; Futter, J. Controlling Preferred Orientation and Electrical Conductivity of Zinc Oxide Thin Films by Post Growth Annealing Treatment. *Appl. Surf. Sci.* **2016**, *367*, 52−58.
(21) Knez, M.; Nielsch, K.; Niinistö, L. Synthesis and Surface Engineering of Complex Nanostructures by Atomic Layer Deposition. *Adv. Mater.* **2007**, *19*, 3425−3438.
(22) Chen, H. C.; Chen, M. J.; Liu, T. C.; Yang, J. R.; Shiojiri, M. Structure and Stimulated Emission of a High-Quality Zinc Oxide Epilayer Grown by Atomic Layer Deposition on the Sapphire Substrate. *Thin Solid Films* **2010**, *519*, 536−540.
(23) Lim, J.; Lee, C. Effects of Substrate Temperature on the Microstructure and Photoluminescence Properties of ZnO Thin Films Prepared by Atomic Layer Deposition. *Thin Solid Films* **2007**, *515*, 3335−3338.
(24) Jeon, S.; Bang, S.; Lee, S.; Kwon, S.; Jeong, W.; Jeon, H.; Chang, H. J.; Park, H.-H. Structural and Electrical Properties of ZnO Thin Films Deposited by Atomic Layer Deposition at Low Temperatures. *J. Electrochem. Soc.* **2008**, *155*, H738−H743.
(25) Lyons, J. L.; Varley, J. B.; Steiauf, D.; Janotti, A.; Van de Walle, C. G. First-Principles Characterization of Native-Defect-Related Optical Transitions in ZnO. *J. Appl. Phys.* **2017**, *122*, 035704.
(26) Niinistö, J.; Mäntymäki, M.; Kukli, K.; Costelle, L.; Puukilainen, E.; Ritala, M.; Leskelä, M. Growth and Phase Stabilization of HfO_2 Thin Films by ALD Using Novel Precursors. *J. Cryst. Growth* **2010**, *312*, 245−249.
(27) Saric, I.; Peter, R.; Piltaver, I. K.; Badovinac, I. J.; Salamon, K.; Petravic, M. Residual Chlorine in TiO_2 Films Grown at Low Temperatures by Plasma Enhanced Atomic Layer Deposition. *Thin Solid Films* **2017**, *628*, 142−147.
(28) Čížek, J.; Valenta, J.; Hruška, P.; Melikhova, O.; Procházka, I.; Novotný, M.; Bulír, J. Origin of Green Luminescence in Hydrothermally Grown ZnO Single Crystals. *Appl. Phys. Lett.* **2015**, *106*, 251902.
(29) Yang, L. L.; Zhao, Q. X.; Willander, M.; Liu, X. J.; Fahlman, M.; Yang, J. H. Origin of the Surface Recombination Centers in ZnO Nanorods Arrays by X-ray Photoelectron Spectroscopy. *Appl. Surf. Sci.* **2010**, *256*, 3592−3597.
(30) Miikkulainen, V.; Leskelä, M.; Ritala, M.; Puurunen, R. L. Crystallinity of Inorganic Films Grown by Atomic Layer Deposition: Overview and General Trends. *J. Appl. Phys.* **2013**, *113*, 021301.
(31) Park, S.-H. K.; Lee, Y. E. Controlling Preferred Orientation of ZnO Thin Films by Atomic Layer Deposition. *J. Mater. Sci.* **2004**, *39*, 2195−2197.
(32) Baji, Z.; Lábadi, Z.; Horváth, Z. E.; Molnár, G.; Volk, J.; Bársony, I.; Barna, P. Nucleation and Growth Modes of ALD ZnO. *Cryst. Growth Des.* **2012**, *12*, 5615−5620.
(33) Kavre Piltaver, I.; Peter, R.; Šarić, I.; Salamon, K.; Jelovica Badovinac, I.; Koshmak, K.; Nannarone, S.; Delač Marion, I.; Petravić, M. Controlling the Grain Size of Polycrystalline TiO_2 Films Grown by Atomic Layer Deposition. *Appl. Surf. Sci.* **2017**, *419*, 564−572.
(34) Fujimura, N.; Nishihara, T.; Goto, S.; Xu, J.; Ito, T. Control of Preferred Orientation for ZnOx Films: Control of Self-Texture. *J. Cryst. Growth* **1993**, *130*, 269−279.
(35) Hesse, R.; Chassé, T.; Szargan, R. Peak Shape Analysis of Core Level Photoelectron Spectra Using UNIFIT for WINDOWS. *Fresenius. J. Anal. Chem.* **1999**, *365*, 48−54.
(36) Kerber, S. J.; Bruckner, J. J.; Wozniak, K.; Seal, S.; Hardcastle, S.; Barr, T. L. The Nature of Hydrogen in X-ray Photoelectron Spectroscopy: General Patterns from Hydroxides to Hydrogen Bonding. *J. Vac. Sci. Technol., A* **1996**, *14*, 1314−1320.
(37) Guziewicz, E.; Godlewski, M.; Wachnicki, L.; Krajewski, T. A.; Luka, G.; Gieraltowska, S.; Jakiela, R.; Stonert, A.; Lisowski, W.; Krawczyk, M.; et al. ALD Grown Zinc Oxide with Controllable Electrical Properties. *Semicond. Sci. Technol.* **2012**, *27*, 074011.
(38) Geng, Y.; Guo, L.; Xu, S.-S.; Sun, Q.-Q.; Ding, S.-J.; Lu, H.-L.; Zhang, D. W. Influence of Al Doping on the Properties of ZnO Thin Films Grown by Atomic Layer Deposition. *J. Phys. Chem. C* **2011**, *115*, 12317−12321.
(39) Ku, C.-S.; Lee, H.-Y.; Huang, J.-M.; Lin, C.-M. Epitaxial Growth of ZnO Films at Extremely Low Temperature by Atomic Layer Deposition with Interrupted Flow. *Mater. Chem. Phys.* **2010**, *120*, 236−239.
(40) Yang, S.; Lin, B. H.; Liu, W.-R.; Lin, J.-H.; Chang, C.-S.; Hsu, C.-H.; Hsieh, W. F. Structural Characteristics and Annealing Effect of ZnO Epitaxial Films Grown by Atomic Layer Deposition. *Cryst. Growth Des.* **2009**, *9*, 5184−5189.
(41) Boichot, R.; Tian, L.; Richard, M.-I.; Crisci, A.; Chaker, A.; Cantelli, V.; Coindeau, S.; Lay, S.; Ouled, T.; Guichet, C.; et al. Evolution of Crystal Structure During the Initial Stages of ZnO Atomic Layer Deposition. *Chem. Mater.* **2016**, *28*, 592−600.
(42) Wójcik, A.; Godlewski, M.; Guziewicz, E.; Minikayev, R.; Paszkowicz, W. Controlling of Preferential Growth Mode of ZnO Thin Films Grown by Atomic Layer Deposition. *J. Cryst. Growth* **2008**, *310*, 284−289.
(43) Murzin, D. Y. On Langmuir Kinetics and Zero Order Reactions. *Catal. Commun.* **2008**, *9*, 1815−1816.
(44) Di Mauro, A.; Cantarella, M.; Nicotra, G.; Privitera, V.; Impellizzeri, G. Low Temperature Atomic Layer Deposition of ZnO: Applications in Photocatalysis. *Appl. Catal., B* **2016**, *196*, 68−76.
(45) Rogé, V.; Bahlawane, N.; Lamblin, G.; Fechete, I.; Garin, F.; Dinia, A.; Lenoble, D. Improvement of the Photocatalytic Degradation Property of Atomic Layer Deposited ZnO Thin Films: The Interplay Between Film Properties and Functional Performances. *J. Mater. Chem. A* **2015**, *3*, 11453−11461.
(46) Megatif, L.; Dillert, R.; Bahnemann, D. W. Reaction Rate Study of the Photocatalytic Degradation of Dichloroacetic Acid in a Black Body Reactor. *Catalysts* **2019**, *9*, 635.
(47) Liu, H. J.; Fan, Z. G.; Li, Y. M. Research on Reaction Kinetics of Photocatalytic Degradation of Methylene Blue in Water Solution with $SrTiO_3$ Nano Film. *Adv. Mater. Res.* **2013**, *662*, 158−162.
(48) Liang, X.; He, Z.; Zhong, Y.; Tan, W.; He, H.; Yuan, P.; Zhu, J.; Zhang, J. The Effect of Transition Metal Substitution on the Catalytic Activity of Magnetite in Heterogeneous Fenton Reaction: In Interfacial View. *Colloids Surf., A* **2013**, *435*, 28−35.
(49) Jang, E. S.; Won, J.-H.; Hwang, S.-J.; Choy, J.-H. Fine Tuning of the Face Orientation of ZnO Crystals to Optimize Their Photocatalytic Activity. *Adv. Mater.* **2006**, *18*, 3309−3312.
(50) Zeng, J. H.; Jin, B. B.; Wang, Y. F. Facet Enhanced Photocatalytic Effect with Uniform Single-Crystalline Zinc Oxide Nanodisks. *Chem. Phys. Lett.* **2009**, *472*, 90−95.
(51) Park, K.-H.; Han, G. D.; Kim, B. J.; Kang, E. H.; Park, J. S.; Shim, J. H.; Park, H.-D. Effects of Atomic Layer Deposition Conditions on the Formation of Thin ZnO Films and Their Photocatalytic Characteristics. *Ceram. Int.* **2019**, *45*, 18823−18830.
(52) Van de Walle, C. G. Hydrogen as a Cause of Doping in Zinc Oxide. *Phys. Rev. Lett.* **2000**, *85*, 1012−1015.
(53) Wang, M.; Jiang, L.; Kim, E. J.; Hahn, S. H. Electronic Structure and Optical Properties of $Zn(OH)_2$: LDA+U Calculations and Intense Yellow Luminescence. *RSC Adv.* **2015**, *5*, 87496−87503.
(54) Vaqueiro-Contreras, M.; Markevich, V. P.; Halsall, M. P.; Peaker, A. R.; Santos, P.; Coutinho, J.; Öberg, S.; Murin, L. I.; Falster, R.; Binns, J.; et al. Powerful Recombination Centers Resulting from Reactions of Hydrogen with Carbon−Oxygen Defects in n-type Czochralski-Grown Silicon. *Phys. Status Solidi* **2017**, *11*, 1700133.
(55) Wang, X.; Huang, H.; Fan, G.; Li, Z.; Zou, Z. Theoretical Insight into Charge-Recombination Center in Ta3N5 Photocatalyst: Interstitial Hydrogen. *J. Phys. Chem. C* **2018**, *122*, 489−494.

https://dx.doi.org/10.1021/acs.jpcc.0c01519
J. Phys. Chem. C XXXX, XXX, XXX−XXX